Structure of β-Purothionin in Membranes: A Two-Dimensional Infrared Correlation Spectroscopy Study†

Julie-Andrée Richard,‡ Isabelle Kelly,‡ Didier Marion,§ Michèle Auger,‡ and Michel Pézolet*,‡

Département de chimie, Centre de Recherche en Sciences et Ingénierie des Macromolécules, Université Laval, Québec, Canada G1K 7P4, and Institut National de la Recherche Agronomique, Unité de recherche sur les protéines végétales et leurs interactions, BP 71627, 44316 Nantes cedex 03, France

Received July 21, 2004; Revised Manuscript Received October 22, 2004

ABSTRACT: Two-dimensional infrared correlation spectroscopy has been used to investigate the structure of β-purothionin, a small basic protein found in the endosperm of wheat seeds, in the absence and presence of dimyristoylphosphatidylglycerol (DMPG) membranes. To generate the two-dimensional synchronous and asynchronous maps, hydrogen−deuterium exchange of the protein amide protons has been used as an external perturbation. This method has allowed us to separate the different secondary structure elements and side chain contributions in the regions of amide I, II, and II′ bands to determine that the relative order of deuteration of the β-purothionin protons is as follows: turns, asparagines, and lysines > unordered structure and tyrosine > β-sheet > α-helices and arginines. The results also indicate that the protein undergoes significant changes both in secondary structure and in deuteration in the presence of DMPG bilayers. The helical content of β-purothionin is higher in the presence of the lipid, and the relative order of deuteration is as follows: lysines and arginines > asparagines and β-sheet > unordered structure and α-helices. The inversion in the deuteration order of the arginine residues is assigned to a change of the degree of association of the protein in the membrane. In addition, the results reveal that the part of the protein containing the tyrosine residue interacts with the lipid membrane. Our results combined with those previously published suggest that the toxicity of β-purothionin is more associated with the formation of functional channels in cell membranes rather than with a lytic phenomenon.

Purothionins are small (∼5 kDa) disulfide-rich basic proteins found in the endosperm of wheat seeds. Three different isoforms of purothionins have been identified, namely, α1-, α2-, and β-purothionin (*1*). Their structure, stabilized by numerous salt bridges, intramolecular hydrogen bonds, and four disulfide bridges, has been determined by NMR spectroscopy (*2*) and X-ray diffraction (*3*, *4*). As crambin, it can be represented by the Greek capital letter Γ. The vertical arm consists of two antiparallel α-helices, and the horizontal one contains a region of extended conformation and a short antiparallel β-sheet (*3*). These proteins have an amphipathic character. The hydrophobic residues are mainly found at the outer surface of the two α-helices, whereas the hydrophilic ones are mainly located at the inner surface of the Γ and at the outer surface of the corner of the Γ (*5*, *6*).

An important feature of all purothionins is their toxicity, which could reflect a direct role in plant defense (*7*). Purothionins appear to be toxic to many organisms such as bacteria, yeast, and fungi (*8*), animals (*9*), cultured mammalian cells (*10*, *11*), and insect larvae (*12*). To determine which characteristics of purothionins are associated with their toxicity, various studies have been performed. Wada et al. (*13*) have proposed the involvement of positive charge in this toxicity. They have observed that a decrease of the positive charge leads to a reduction of the toxicity, in proportion to the number of modified groups. It has also been demonstrated that crambin, which has no positive charge unlike the other thionins, does not show any toxicity to various organisms (*6*, *14*). The single tyrosine residue present in purothionins is also believed to play a major role in the toxicity. When it is chemically modified (nitration or iodination), a decrease, even a loss, of the toxicity is observed (*13*). On the basis of these observations, it has been concluded that the positive charge of the protein plays an important role in the interaction with the negatively charged cell surface and that the toxicity of purothionins depends on the state of the tyrosine residue (*13*).

It was shown that the toxicity of purothionins is mainly based on the formation of ion channels in membranes. The formation of these channels has been suggested from studies of natural membranes as in myelinated axons (*15*), C2 myotubes, and mammalian neuromuscular junctions (*16*). The ion channel properties of these proteins have been studied using electrophysiology techniques on model lipid membranes composed of natural phospholipids. Purothionins form single channels whose ionic selectivity is $Na^+ \sim K^+$

† This work was supported by the Natural Science and Engineering Research Council (NSERC) of Canada, by the Fonds Québécois pour la Recherche sur la Nature et les Technologies from the province of Québec, and by the Centre de Recherche en Sciences et Ingénierie des Macromolécules. J.-A.R. also thanks NSERC for the award of a postgraduate scholarship.

* To whom correspondence should be addressed. Phone: (418) 656-2481. Fax: (418) 656-7916. E-mail: michel.pezolet@chm.ulaval.ca.

‡ Université Laval.

§ Institut National de la Recherche Agronomique.

10.1021/bi048443t CCC: $30.25
Published on Web 12/10/2004

$\gg Cl^-$ for the low-conductance channels and $Cl^- \gg Na^+$ for the high-conductance channels, indicating that they correspond to cationic and anionic channels, respectively (*17*, *18*). To understand the formation of these channels, the interaction between purothionins and lipid membranes has been investigated by several groups. Huang et al. (*19*) have studied the interaction between *Pyrularia* thionin, an analogue of purothionins, and large unilamellar vesicles (LUV) of dipalmitoylphosphatidylglycerol (DPPG)[1] by differential scanning calorimetry (DSC). This study suggests that the interaction between the thionin and the lipid could involve a two-step mechanism. First, the protein adsorbs to the bilayer surface through electrostatic interactions and then penetrates the hydrophobic bilayer region through a mechanism driven by the thionin tryptophan. The interaction between DMPG bilayers and β-purothionin has been investigated by ^{31}P NMR and infrared spectroscopy (*20*). The results indicate that the organization of the lipid bilayer is not significantly affected by the presence of β-purothionin and that the protein decreases the rate of lateral diffusion of DMPG. On the other hand, the results also demonstrate the existence of an electrostatic interaction between DMPG and β-purothionin and a partial insertion of the protein in the lipid membrane.

Infrared spectroscopy has been widely used to study the secondary structure of proteins from the analysis of the amide bands. More specifically, the shape and frequency of the bands due to the amide A ($\sim$3300 cm^{-1}), I ($\sim$1650 cm^{-1}), II ($\sim$1550 cm^{-1}), and III ($\sim$1400−1200 cm^{-1}) vibrations have been shown to be sensitive to the protein secondary structure. However, a main limitation of this technique is that the amide bands due to the different secondary structure elements (α-helices, β-sheets, turns, and unordered structure) strongly overlap so that the analysis of amide bands is often difficult. Fortunately, resolution enhancement tools such as Fourier deconvolution allow to distinguish the components present under broad absorption bands and to discriminate between secondary structures (*21*−*24*).

More recently, Noda has developed a spectral analysis method called two-dimensional correlation spectroscopy (*25*, *26*). The aim of this technique is to emphasize in-phase and out-of-phase correlations between spectral intensity variations occurring at different wavenumbers that are induced by the application of an external perturbation on the studied system. Although two-dimensional (2D) correlation spectroscopy has first been introduced in the study of the dynamic spectra generated by small-amplitude deformation of polymers (*27*, *28*), Noda proposed in 1993 a generalized formalism allowing one to produce synchronous or asynchronous 2D correlation maps from systematic variations of spectra induced by different types of external perturbations and waveforms (*26*). The main advantage of this technique is that it allows an enhancement of the spectral resolution by spreading the overlapping bands over a second dimension (*28*). In addition, from the analysis of the sign of the correlation peaks in the 2D maps, this technique may allow a better band assignment and the establishment of a sequence of events during a physical or chemical process.

[1] Abbreviations: DMPG, dimyristoylphosphatidylglycerol; 2D-IR, two-dimensional infrared; ATR, attenuated total reflection; H/D, hydrogen−deuterium.

Several studies on proteins and peptides have been realized using two-dimensional infrared (2D-IR) correlation spectroscopy. For example, 2D-IR spectroscopy has allowed the investigation of correlations between amide I, amide II, or amide III bands (*29*, *30*) or between bands in the mid- and near-IR regions (*31*−*33*). It has also been extensively used to gain insight into the sequence of events occurring during protein denaturation induced by temperature (*34*−*39*), pressure (*40*), or pH (*41*). Finally, it has also been applied to the analysis of the kinetics of the hydrogen−deuterium exchange of protein amide protons to obtain information about the solvent accessibility of protein secondary structure elements (*29*, *30*, *42*, *43*). One important advantage of the last technique is that the use of different exchange time domains can be very efficient in separating fast and slow kinetics (*29*).

In this study, we have studied the structure of β-purothionin by 2D-IR spectroscopy using hydrogen−deuterium exchange as the external perturbation. Its secondary structure and the deuteration order of the different structure elements have been determined in the absence and presence of a model lipid membrane of dimyristoylphosphatidylglycerol, an anionic lipid found in the cellular membrane of bacteria. Since the three-dimensional structure of β-purothionin is already known (*3*), the study of its structure by 2D-IR spectroscopy is useful in verifying the efficiency of 2D-IR spectroscopy coupled with hydrogen−deuterium exchange to study the conformation of the protein and the accessibility of the amide bonds. This method has also allowed us to determine which part of the protein interacts with the lipid membrane.

EXPERIMENTAL PROCEDURES

Materials. Dimyristoylphosphatidylglycerol (DMPG) was purchased from Avanti Polar Lipids (Alabaster, AL) and used without further purification. β-Purothionin has been extracted and purified as described previously (*20*).

Methods. For the study of β-purothionin, approximately 250 μg of protein in solution [5 μL at 5% (w/v) in a 150 mM NaCl solution (pH 7.0)] was deposited on an attenuated total reflection (ATR) germanium crystal (50 mm × 20 mm × 2 mm, 45°), dried, and placed in a sealed cell in which a stream of nitrogen, bubbling in D_2O (CDN Isotopes, Pointe Claire, PQ), was passed continuously over the surface of the crystal to carry out the deuteration. For the study of the DMPG−β-purothionin complex, a dispersion containing 10% (w/v) of the phospholipid in a 150 mM NaCl solution was prepared by heating this dispersion at a temperature of 40 °C and cooling it in liquid nitrogen. This cycle was repeated five times. The pH was adjusted to 7.0. Volumes of the β-purothionin solution and the DMPG dispersion were then mixed to obtain a lipid:protein molar ratio of 30:1. Then, 40 μL of the complex was deposited on a germanium crystal, dried, and placed in the sealed cell. All spectra were recorded with a Nicolet Magna 550 spectrometer equipped with a narrow-band MCT detector. A total of 250 scans were averaged for the reference spectrum and 16 scans for the sample at a resolution of 2 cm^{-1}. For each experiment, 350 successive 16-scan spectra were recorded. The 1380−1720 cm^{-1} region was truncated and corrected for the baseline using a straight line for β-purothionin and a fourth-order polynomial for the lipid−protein complex. Deconvolved amide I bands were obtained using the technique of Griffiths

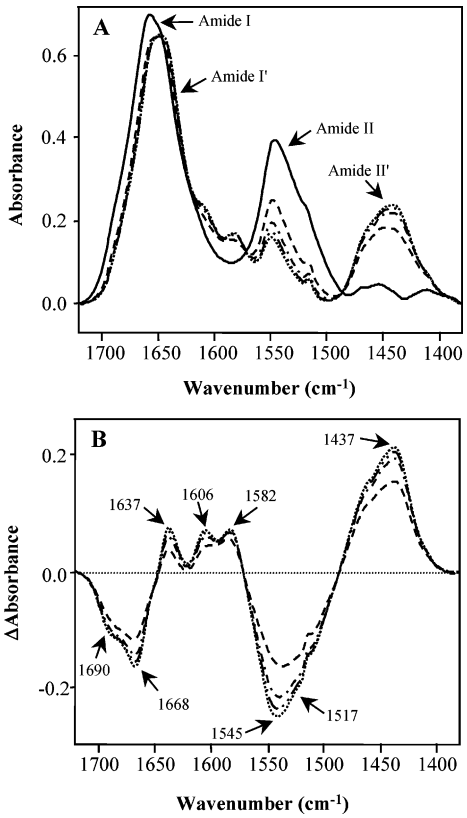

FIGURE 1: (A) ATR and (B) difference infrared spectra of β-purothionin as a function of the deuteration time: (—) 0, (- - -) 15, (— - —) 30, (— - - —) 40, and (•••) 50 min.

and Pariente (*44*), with a narrowing parameter (γ) of 5.45 and a smoothing parameter of 75% for the pure protein and 81% for the lipid−protein complex. All spectral manipulations were performed with Grams (Thermo-Galactic Industries Corp., Salem, NH).

Synchronous and Asynchronous Correlation Calculations. Two-dimensional synchronous (Φ) and asynchronous (Ψ) correlation maps were calculated using the generalized formalism of Noda (*26*) as described by Nabet and Pézolet (*29*). The dynamic spectra used for the calculations were obtained by subtracting from each spectrum of the series the spectrum recorded just before the beginning of the deuteration process. For both β-purothionin and the lipid−protein complex, the correlation calculations were carried out using the 36 spectra recorded during the first 15 min of deuteration. In the case of pure β-purothionin, calculations were also carried out using the 22 spectra recorded after deuteration for 50−58 min. All these calculations were carried out using Mathcad 7 (MathSoft Inc., Cambridge, MA). 2D correlation maps were plotted using the visualization software Transform (Research Systems Inc., Boulder, CO).

RESULTS AND DISCUSSION

Deuteration of β-Purothionin

ATR Spectra. Figure 1A shows a series of infrared ATR spectra of β-purothionin recorded as a function of the deuteration time. As can be seen, upon H−D exchange, the intensity and position of the amide bands are strongly affected. The most intense absorption band occurs near 1660 cm^{-1} and is due to the amide I vibration. Since this vibration involves mostly the stretching of the amide C=O group (70−85%) (*45*), the amide I band shifts by only ~10 cm^{-1} toward lower wavenumbers after H−D exchange. On the other hand, the amide II band, which is mainly due to the in-plane N−H bending vibration (40−60%) coupled with the C−N stretching vibration (18−40%) of the peptide bond (*45*), shifts by ~100 cm^{-1} toward lower wavenumbers by the H−D exchange. Spectra of Figure 1A also reveal the presence of two bands at 1606 and 1582 cm^{-1} that increase in intensity with time. These bands are due to the asymmetric and symmetric vibrations of C−N bonds of the guanidinium group of the arginine residues that shift upon deuteration from 1633 and 1673 cm^{-1} to 1606 and 1582 cm^{-1}, respectively (*46*, *47*).

Figure 1B shows the difference spectra obtained as a function of deuteration time, by subtracting from each spectrum of Figure 1A the spectrum recorded just before the beginning of the deuteration process. As can be seen, the spectral changes occurring upon H−D exchange are more clearly seen in panel A. The changes observed are due to the shift to a lower wavenumber of the amide I and II vibrations of the different secondary sructures as well as of vibrations of some side chains. Since some of these bands are broad and unresolved, it is difficult to assign them unambiguously. For example, the broad negative band with minima at 1690 and 1668 cm^{-1} could be assigned to the superposed decrease in the intensity of the amide I bands of amide groups involved in β-sheets (the high-frequency component occurring around 1690 cm^{-1}), and in other secondary structures such as turns, unordered structure, and helices (*21*, *42*, *45*, *48*) as well as to the decrease in the intensity of bands due to the arginine (1673 cm^{-1}) and asparagine (1678 cm^{-1}) side chains (*46*). The positive band at 1637 cm^{-1} is assigned to the amide I′ vibration since its intensity increases with deuteration. As in Figure 1A, the two bands due to the arginine residues at 1606 and 1582 cm^{-1} are clearly observed in the difference spectra. In addition, it is easily seen that the intensity of the amide II band around 1545 cm^{-1} decreases while that of the amide II′ band (1437 cm^{-1}) increases during the deuteration process. Finally, the small shoulder observed at 1517 cm^{-1} on the negative amide II band is due to the deuteration of the single tyrosine residue of β-purothionin (*47*).

The percentage of amide protons that are exchanged during the deuteration can be determined as a function of time from the ratio of the areas of amide II and amide I bands. As seen in Figure 2, the amide II:amide I intensity ratio indicates that ~90% of the amide protons of β-purothionin (□) are exchanged after deuteration for 200 min. Figure 2 also reveals that the kinetics of the deuteration process is very fast at the beginning and slows after deuteration for ~15 min.

2D-IR Spectra. The deuteration of β-purothionin has been studied for two time domains: one at the beginning of the deuteration process (0−15 min), to follow the rapidly exchanging protons, and a second one after 50 min (50−58 min), to probe the slowly exchanging amide groups. These time domains are highlighted on the deuteration curve shown in Figure 2. Figure 3 shows the synchronous (Φ) and the asynchronous (Ψ) correlation maps obtained for β-purothionin for the first 15 min of deuteration. On the synchronous map, autopeaks appear only when the corresponding infrared

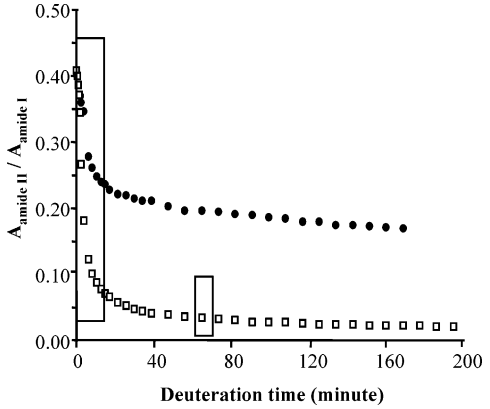

FIGURE 2: Kinetics of deuteration for β-purothionin (□) and the DMPG−β-purothionin (●) complex. The time regions studied by 2D-IR spectroscopy are boxed.

bands are modified by deuteration, such as the amide I (1670 cm^{-1}), II (1534 cm^{-1}), and II′ (1437 cm^{-1}) bands. On the other hand, the sign of the cross-peaks allows us to determine the relative direction between the spectral variations. A positive cross-peak will appear if two variations are in the same direction (the intensity of two bands increases or decreases simultaneously), and a negative cross-peak will appear if two variations are in opposite directions (one band increases in intensity while the other one decreases). The strongest peak of the synchronous map is observed in the amide II and amide II′ regions at 1534 and 1437 cm^{-1}, respectively, since the amide II vibration is much more strongly affected by the deuteration of the amide groups than the amide I vibration. The negative cross-peak observed at 1534 and 1437 cm^{-1} is due to the fact that the amide II band at 1534 cm^{-1} is replaced by the amide II′ band at 1437 cm^{-1} upon deuteration of the amide protons. However, the synchronous map in the amide II and amide II′ region does not display a clearly resolved spectral contribution for the different conformations present in the protein. The presence of a negative cross-peak at 1635 cm^{-1} correlated with the 1660−1700 cm^{-1} amide I region indicates that this feature is due to the amide I′ vibration and is most likely due to the deuteration of the β-sheet strand of β-purothionin (*21*).

As seen in Figure 3, the asynchronous correlation map contains several well-resolved peaks showing that indeed the resolution is enhanced in 2D-IR spectroscopy. Asynchronous peaks develop only if the variation of the spectral intensities at wavenumbers $\bar{\nu}_1$ and $\bar{\nu}_2$ are out-of-phase (i.e., delayed or accelerated). Noda has shown that by combining the sign of the peaks in the synchronous and asynchronous maps, it is possible to determine the sequence of the spectral variations (*26*). Table 1 summarizes the main correlation peaks observed in the asynchronous map of Figure 3, their assignment based on the existing literature on infrared spectroscopy of proteins and amino acids and the chronological order of deuteration of each component of the correlation peaks. As can be seen, the calculation of the asynchronous correlation maps results in a significant increase of the spectral resolution as first mentioned by Noda (*26*, *28*). For example, several peak maxima are observed in the amide I region between 1600 and 1700 cm^{-1}. Peaks at 1677, 1666, and 1625 cm^{-1} are assigned to the three asparagine, four arginine, and six lysine side chains, respectively (*46*). The peaks at 1635 and 1700 cm^{-1} are assigned to the β-sheet structure, while turns and unordered structures give rise to peaks at 1670 and 1656 cm^{-1}, respectively (*21*). From the sequence of deuteration of the different peaks listed in Table 1, one can conclude that turns and asparagine and lysine side chains are the first elements to be deuterated. The characteristic wavenumber positions of turns are 1670 cm^{-1} in the amide I region and 1443 cm^{-1} in the amide II′ region. Those of lysine residues are 1628 and 1531 cm^{-1} and are due to the asymmetric bending vibrations of the lysine NH_3^+ groups (*46*). In the tertiary structure of β-purothionin shown in Figure 4, turns and lysine residues are localized in accessible regions, four lysine residues of six being found in turns and unordered structure. The accessibility of these amide and side chain protons could explain why they are rapidly exchanged. The unordered structure is the next one to be deuterated, and its characteristic wavenumbers are 1656, 1540, and 1454 cm^{-1}. The absence of regular hydrogen bonds for this secondary structure most likely allows the amide protons to be exchanged more easily than those of α-helices or β-sheets.

In the 2D asynchronous map, the peak at 1517 cm^{-1} is assigned to the tyrosine residue (*47*). The exchange rate of the tyrosine appears to be similar to that of the amide protons of the unordered conformation. The cross-peak associated with this amino acid is quite strong even though there is only one tyrosine residue in β-purothionin. The presence of this cross-peak shows that the proton of the tyrosine residue is easily exchanged even though it is buried in the pair of α-helices (Figure 4) (*3*). Results obtained by visible Raman spectroscopy have also shown that tyrosine 13 of α1-purothionin is hydrogen bonded to water molecules (*49*). On the other hand, from the results obtained with ultraviolet resonance Raman spectroscopy, it was suggested that the tyrosine residue of both α1- and β-purothionins is constrained in a hydrophobic pocket (*50*). The peak at 1507 cm^{-1} could be due to the presence of tyrosinate since it has been shown that the ionization of the tyrosine hydroxyl group results in the shift of the 1517 cm^{-1} band toward a lower wavenumber (*45*, *47*). However, results obtained by fluorescence spectroscopy have shown that α- and β-purothionins contain no significant ground-state tyrosinate and that the 345 nm fluorescence emission is generated by excited-state proton transfer (*51*). The precise assignment of the 1507 cm^{-1} band is thus still unclear.

The β-sheet is the third secondary structure to be deuterated. The wavenumber positions associated with this structure are 1700, 1635, 1531, and 1443 cm^{-1} (*21*). β-Sheet protons are more difficult to exchange than those of unregular structures because of the presence of strong hydrogen bonds in β-sheets. The latest protons to be exchanged during the initial deuteration period are those of the backbone of the α-helices and of the arginine side chains. The amide II vibration of the α-helices appears at 1544 cm^{-1}, while the amide II′ band is observed near 1433 cm^{-1} (*21*). No characteristic peaks due to the α-helices are observed in the amide I region on this asynchronous map. As for the β-sheet, the presence of hydrogen bonds in α-helices explains why the deuteration is slower than for the other structures. Peaks due to arginine side chains are observed at 1666 cm^{-1} for the nondeuterated side chains and at 1580 and 1602 cm^{-1} for the deuterated ones. According to the crystal structure of β-purothionin (Figure 4), the arginine residues at positions

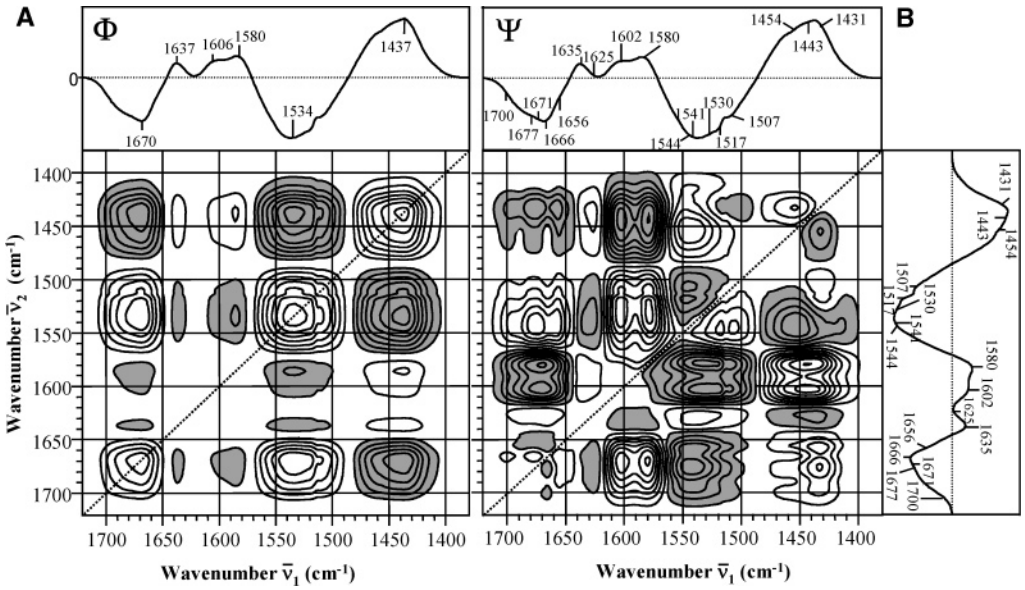

FIGURE 3: (A) Synchronous and (B) asynchronous 2D correlation spectra of β-purothionin obtained for the first 15 min of deuteration. The white peaks are positive, and the gray peaks are negative. The spectra above the correlation maps are the difference spectra (final spectrum − initial spectrum). The intensities of the peaks in the asynchronous map are on the order of 2% of those in the synchronous map.

Table 1: Assignment[a] of the Cross-Peaks Found on the Asynchronous Correlation Map of Figure 3 (α, α-helices; β, β-sheet; t, turns; u, unordered structure)

region	faster exchanging component (cm^{-1})	slower exchanging component (cm^{-1})
amide I−amide I	1677 (Asn)	1666 (Arg)
	1700 (β)	1666 (Arg)
	1656 (u)	1666 (Arg)
	1625 (Lys)	1666 (Arg)
	1670 (t)	1580 (Arg)
	1670 (t)	1602 (Arg)
	1635 (β)	1580 (Arg)
	1635 (β)	1602 (Arg)
amide II−amide II	1517 (Tyr)	1544 (α)
	1507 (tyrosinate?)	1544 (α)
	1531 (β and Lys)	1580 (Arg)
	1531 (β and Lys)	1602 (Arg)
amide I−amide II	1628 (Lys)	1540 (u)
	1676 (Asn)	1540 (u)
amide II′−amide II′	1454 (u)	1433 (α)
amide II−amide II′	1507 (tyrosinate?)	1433 (α)
	1454 (u)	1544 (α)
	1443 (t or β)	1580 (Arg)
	1443 (t ot β)	1602 (Arg)
amide I−amide II′	1628 (Lys)	1433 (α)
	1656 (t)	1433 (α)
	1676 (Asn)	1433 (α)

[a] From refs *21*, *28*−*31*, *40*, *45*−*48*, and *61*−*63*.

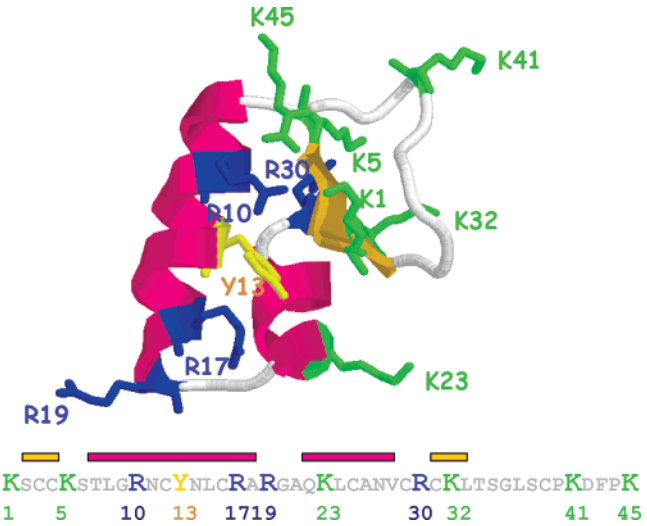

FIGURE 4: Primary and three-dimensional structure of β-purothionin showing the location of the two α-helices (red) and of the β-sheet (yellow). The structure was designed using Rasmol from the crystal data deposited in the Protein Data Bank (entry 1HBP). The single tyrosine (yellow) residue and the lysine (green) and arginine (blue) residues are also highlighted in both the one- and three-dimensional structures.

10 and 17 are constrained in helix H1 and should be less accessible to H−D exchange (*4*).

From these results, we can therefore conclude that the relative order of deuteration of the β-purothionin protons is as follows: turns, asparagines, and lysines > unordered structure and tyrosine > β-sheet > α-helices and arginines. This is in good agreement with structural data showing that turns and most lysine residues are exposed to the solvent while the antiparallel helices containing half of the arginine residues are strongly packed together to form a bundle (Figure 4). Furthermore, in the crystal lattice, packing of the protein molecules in tetramers involves leucine−ladder type interactions between the first helices of two proteins and also the two arginines found in these helices (*3*). Since, in our study, the protein solution is first spread and dried on the germanium ATR crystal, it appears that the structure obtained is similar to that in single crystals. The relatively good accessibility of the tyrosine residue to deuteration is in good agreement with the fact that this residue plays a key role in the toxicity of purothionin and in the interaction with lipid membranes (*13*).

To confirm that the amide protons of the α-helices are among the last ones to be exchanged, 2D correlation maps were calculated using a series of spectra recorded at a longer deuteration time. Figure 5 shows the synchronous and asynchronous maps obtained from the spectra recorded after deuteration for 50−58 min. As can be seen, these maps are strikingly different from those shown in Figure 3. On the synchronous correlation map, an autopeak is observed at

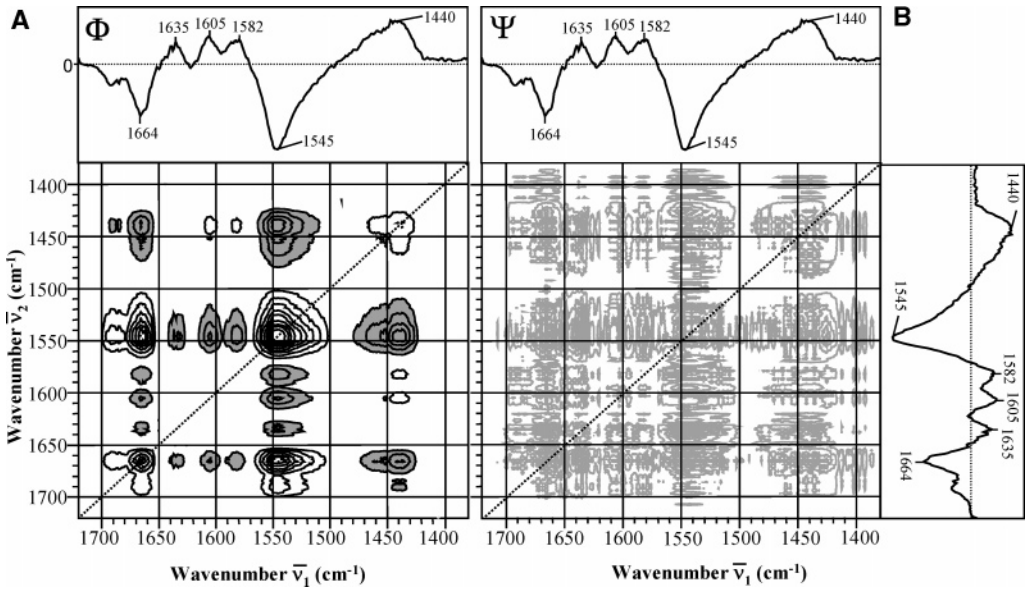

FIGURE 5: (A) Synchronous and (B) asynchronous 2D correlation spectra of β-purothionin obtained after deuteration for 50−58 min. The white peaks are positive, and the gray peaks are negative. The spectra above the correlation maps are the difference spectra (final spectrum − initial spectrum). The intensities of the peaks in the asynchronous map are on the order of 1.5% of those in the synchronous map.

1664 cm^{-1} that we assigned to the deuteration of the α-helices. Although this wavenumber is high compared to those normally found in the literature [∼1650−1655 cm^{-1} (*21*, *52*)], it is known that shorter helices give rise to amide I bands at higher wavenumbers (*45*). For example, helices containing 8−10 residues and 5−7 residues should have amide I bands at 1663 and 1668 cm^{-1}, respectively. This is the case for β-purothionin where the two antiparallel helices are composed of 12 (residues 7−18) and 7 residues (residues 22−28) as shown in Figure 4. Furthermore, it has been found that the amide I band due to the α-helices of proteins such as rhodopsin and bacteriorhodopsin are located at 1665 (*53*) and 1659 cm^{-1} (*54*, *55*), respectively. It is therefore reasonable to assign the peak found at 1664 cm^{-1} to α-helices. In Figure 5, we can also see that the amide II band is centered at 1545 cm^{-1} compared to 1534 cm^{-1} (see Figure 3) at the beginning of the deuteration process. The amide II band is thus shifted toward higher wavenumbers, approaching those attributed to the α-helices [∼1550 cm^{-1} (*21*, *45*)].

Cross-peaks associated with the arginine side chains are also observed at 1605 and 1582 cm^{-1} on the 2D synchronous map of Figure 5. The fact that the arginine side chains are still deuterated after 50 min could be explained by their distributions along the structure of β-purothionin. Figure 4 shows that two arginine residues are in helix H1 (arginines 10 and 17) while the two others are in turns well exposed to the solvent (arginines 19 and 30) (*3*). Thus, the most accessible arginines would be exchanged first, whereas the arginines less accessible and stabilized by intramolecular bonds would be exchanged later. This hypothesis could explain why the cross-peaks of arginine side chains are present all along the deuteration process.

Figure 5 shows that the asynchronous correlation map calculated after deuteration for 50 min is essentially devoided of significant cross-peaks, thus revealing that the protons of α-helices and of arginine side chains are exchanged at the same rate. A weak and noisy asynchronous correlation map has also been observed by Nabet and Pézolet (*29*) for myoglobin after deuteration for 1 h.

These results clearly show that valuable information about the accessibility of the amide group and side chain protons can be obtained from the combined used of 2D-IR spectroscopy and H−D exchange.

Deuteration of the DMPG−β-Purothionin Complex

ATR Spectra. Figure 6A shows a series of infrared ATR spectra of the DMPG−β-purothionin complex (30:1 molar ratio) recorded as a function of the deuteration time. As for the pure protein (Figure 1A), the amide I, II, and II′ bands are affected by H−D exchange but to a lesser extent. Indeed, the amide I band shifts by only ∼2 cm^{-1} toward lower wavenumbers compared to 10 cm^{-1} for pure β-purothionin. In addition, the curve for the H−D exchange kinetics obtained for the DMPG−β-purothionin complex [Figure 2 (●)] shows that the deuteration level achieved in the case of the complex is lower than that of β-purothionin. Indeed, the ratio of the areas of the amide II and amide I bands indicates that only 50% of the protein amide protons are exchanged after deuteration for 150 min for the complex compared to 90% for pure β-purothionin. Therefore, the presence of DMPG partially prevents the exchange of the amide protons of β-purothionin, suggesting that some parts of the protein interact with the DMPG membrane. To emphasize the spectral changes induced by the deuteration, the difference spectra obtained by subtracting from the spectra of Figure 6A the spectrum recorded just before the beginning of the deuteration are plotted as a function of the deuteration time in Figure 6B. The most interesting feature of these spectra is that the main bands affected by the H−D exchange are those of arginine side chains at 1610 and 1584 cm^{-1}. This suggests that when the protein is bound to DMPG, it adopts a position relative to the membrane or has a different tertiary structure, resulting in an increased level of deuteration of the arginine side chains.

Another interesting feature seen in Figure 6A is that the shape of the amide I band for the lipid−protein complex is different from that of β-purothionin in the absence of lipid (Figure 1A). Indeed, there are clearly two components for

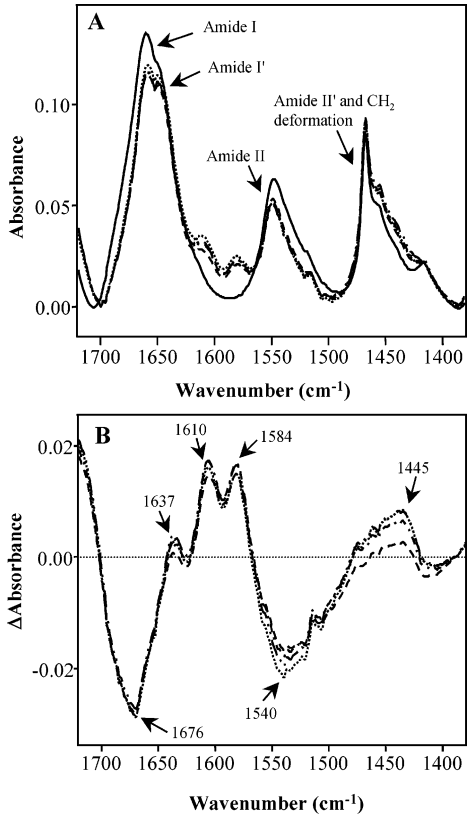

FIGURE 6: (A) ATR and (B) difference infrared spectra of the DMPG−β-purothionin complex (30:1 molar ratio) as a function of the deuteration time: (—) 0, (- - -) 15, (— - —) 30, (— - - —) 40, and (•••) 50 min.

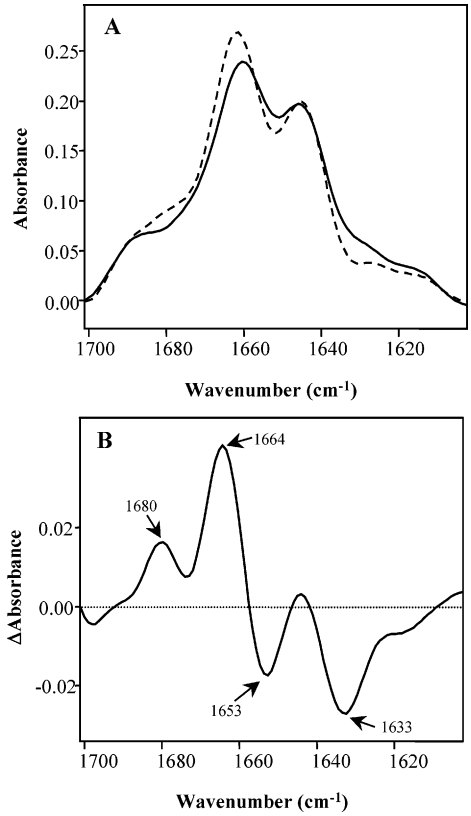

FIGURE 7: (A) Deconvolved infrared spectra in the region of the amide I band for β-purothionin (—) and for the DMPG−β-purothionin complex (- - -). (B) Difference between the infrared spectra of the DMPG−β-purothionin complex and β-purothionin before the deuteration process.

the protein in the presence of DMPG, suggesting a perturbation of the secondary structure. To emphasize these changes, the amide I bands of β-purothionin recorded just before the beginning of the deuteration in the absence and presence of DMPG were Fourier deconvolved. The resulting spectra presented in Figure 7A show that the intensity of the component at 1664 cm^{-1}, assigned to the α-helices, relative to that of the β-sheet band at 1633 cm^{-1} is higher when β-purothionin is bound to DMPG. For a better comparison of these two spectra, the difference spectrum was calculated by subtracting the spectrum of β-purothionin from that of the complex. As can be seen in Figure 7B, the interaction of DMPG and β-purothionin results in the clear increase in the absorbance of the band at 1664 cm^{-1} assigned above to short helices at the expense of that of the 1653 cm^{-1} band, usually assigned to α-helices (*21*, *52*) and of the β-sheet band at 1633 cm^{-1}. This result reveals that the secondary structure of β-purothionin is affected by the presence of DMPG and that two different populations of α-helices may be present in the lipid−protein complex.

2D-IR Spectra. To obtain more information about the interaction between the protein and DMPG and about the structure of the bound protein, we have studied the DMPG−β-purothionin complex by 2D-IR correlation spectroscopy. Figure 8 shows the correlation maps obtained for the first 15 min of the deuteration process. The synchronous correlation map is similar to the correlation map presented in Figure 3 for the pure protein and leads to the same interpretation concerning the relative order of spectral variations. However, the relative intensity of some of the peaks is strikingly different. For example, the doublet at 1610 and 1584 cm^{-1} due to the arginine guanidinium dominates the synchronous map of the lipid−protein complex, while the correlation peaks between the amide II (1540 cm^{-1}) and amide II′ (1445 cm^{-1}) bands are much weaker. Moreover, the peak at 1635 cm^{-1} assigned to the amide I′ vibration of the β-sheet is absent. All these observations are in agreement with the ATR difference spectra shown in Figure 6, namely, that deuteration is less important for the DMPG−β-purothionin complex and that the deuteration of the arginine residues is easier when the protein is bound to the lipid membrane. This suggests that the protein interacts with the lipid bilayer in such a way that the accessibility of the guanidinium protons of the arginines is enhanced compared to that of the pure protein, thus facilitating the deuteration of the arginine side chains. This could be due to a difference between the state of association of the protein in the presence of phospholipids and in the solid state. The crystal structure of β-purothionin shows that the protein molecules associate into clusters and can form tetramers stabilized by hydrophobic and hydrophilic interactions (*3*). The binding of the protein to DMPG could lead to the disruption of this cluster association, making some arginine residues more exposed to the solvent, especially arginines 10 and 17 of helix H1 (Figure 4). The binding with the DMPG membrane could also cause a partial opening of the β-purothionin structure, favoring the exchange of the guanidinium protons.

The asynchronous correlation map presented in Figure 8 contains fewer cross-peaks than that presented in Figure 3 for the pure protein. This suggests that the interaction of the protein with the lipid membrane prevents the exchange of

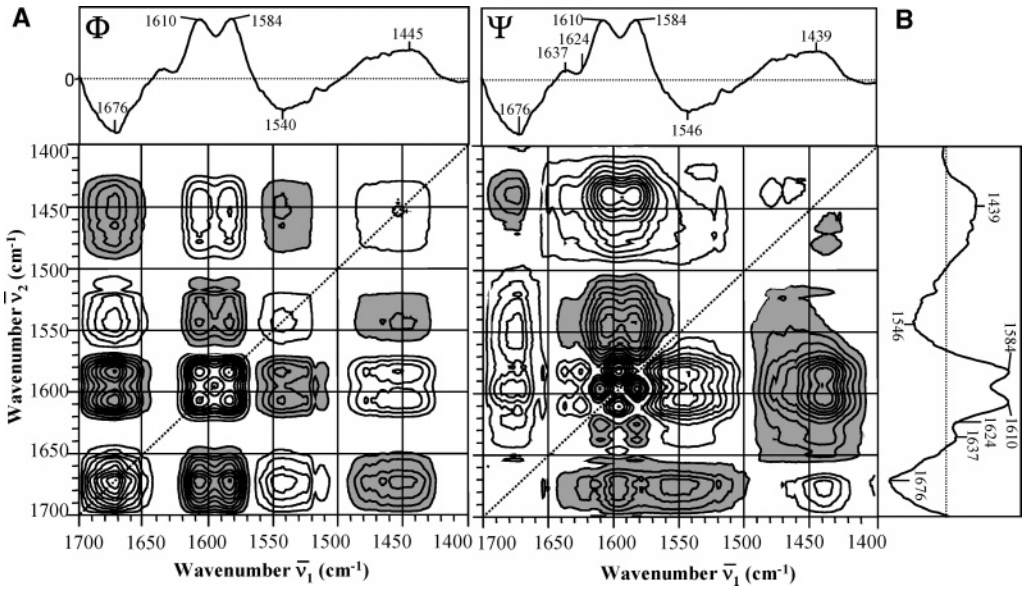

FIGURE 8: (A) Synchronous and (B) asynchronous 2D correlation spectra of the DMPG−β-purothionin complex obtained for the first 15 min of deuteration. The white peaks are positive, and the gray peaks are negative. The spectra above the correlation maps are the difference spectra (final spectrum − initial spectrum). The intensities of the peaks in the asynchronous map are on the order of 2% of those in the synchronous map.

Table 2: Assignment[a] of the Cross-Peaks Found on the Asynchronous Correlation Map of Figure 8 (α, α-helices; β, β-sheet; t, turns; u, unordered structure)

region	faster exchanging component (cm^{-1})	slower exchanging component (cm^{-1})
amide I−amide I	1624 (Lys)	1610 (Arg)
	1624 (Lys)	1582 (Arg)
	1610 (Arg)	1637 (β)
	1582 (Arg)	1639 (β)
	1595 (Arg)	1675 (Asn)
amide II−amide II	1582 (Arg)	1546 (α)
	1602 (Arg)	1544 (α)
amide I−amide II	1676 (Asn)	1549 (α)
amide II−amide II′	1586 (Arg)	1439 (α or u)
	1602 (Arg)	1439 (α or u)
amide I−amide II′	1676 (Asn)	1438 (α or u)

[a] From refs *21* and *45*−*47*.

protons of some amino acids and secondary structures. Table 2 presents the assignment of the cross-peaks observed in the asynchronous map of the DMPG−β-purothionin complex and the chronological order of deuteration of each component of the correlation peaks. The arginine−arginine cross-peaks observed at 1595 and 1582 cm^{-1} and at 1595 and 1611 cm^{-1} are not included in this table since we believe that these weak peaks are not due to specific arginine residues but rather to a change of the width of the arginine bands with deuteration. Spectra simulations performed by Czarnecki (*56*) as well as in our laboratory (*57*) have shown that small change in width for strong synchronous bands can give rise to such a regular pattern in the asynchronous maps. The results of Table 2 show that the arginine and lysine residues are the first components to be exchanged. However, unlike in the asynchronous correlation map of the protein in the absence of lipid (Figure 3), the peaks due to the lysine residues are much weaker. Since these residues are positively charged, it is likely that they interact with the negatively charged DMPG molecules, therefore limiting the exchange of their protons. The interaction between the negatively charged cell surface and the purothionin lysine residues has already been suggested by Wada et al. (*13*). Furthermore, infrared and NMR spectroscopy results have shown that the electrostatic interactions between β-purothionin and DMPG at high lipid: protein molar ratio result in the decrease of the extent of lateral diffusion of the lipid in the fluid phase and in the increase in the gel-to-fluid phase transition temperature (*20*).

The asynchronous correlation map also indicates that the H−D exchange next affects the asparagines and the β-sheet. Finally, the last structures to be exchanged are the unordered structure and the α-helices. The fact that the unordered structure is one of the last structures to be deuterated, even though it is not involved in hydrogen bonds, suggests that this part of the protein interacts with the lipid membrane. From these results, we can therefore conclude that the relative order of deuteration of β-purothionin bound to DMPG is as follows: lysines and arginines > asparagines and β-sheet > unordered structure and α-helices. An interesting feature of the asynchronous correlation map is the absence of the cross-peak associated with the tyrosine residue at 1517 cm^{-1}. This is in agreement with previous studies that have suggested an interaction between the tyrosine residue of β-purothionin and lipid membranes (*3*, *13*, *58*).

CONCLUSIONS

2D-IR correlation spectroscopy with hydrogen−deuterium exchange as the external perturbation was used in this study to investigate the structure of β-purothionin in the absence and presence of DMPG and to determine the chronological sequence of the deuteration of the different conformations and of some of the side chains. For the protein alone, the relative order of deuteration is as follows: turns, asparagines, and lysines > unordered structure and tyrosine > β-sheet > α-helices and arginines. In the presence of DMPG bilayers, the level of deuteration of β-purothionin is significantly reduced and the arginine residues are the first structural elements to be exchanged. The relative order of deuteration then becomes the following: lysines and arginines > asparagines and β-sheet > unordered structure and α-helices.

Furthermore, no correlation peak due to the tyrosine residue was observed for the lipid−protein complex, suggesting that the part of the proteins containing the tyrosine residue interacts with the negatively charged DMPG membrane. The results also indicate that there is an increase in the α-helix content of β-purothionin upon binding to the lipid membrane.

These significant differences observed in the deuteration of amide bonds and side chains upon lipid binding suggest a significant change in the protein structure and in the degree of association of the protein molecules. Previous NMR and infrared results have shown that the bilayer structure of DMPG is not significantly affected by β-purothionin and that electrostatic interactions exist between the lipid and the protein (*20*). These results also demonstrated that the protein is partially inserted into the lipid membrane, the α-helices and the β-sheet having tilt angles of approximately 60° and 30°, respectively, relative to the bilayer normal. The insertion of the protein in the membrane could lead to the formation of hydrophilic channels to allow the passage of ions and water molecules as suggested from electrophysiology measurements on natural membranes (*15*, *16*). Since the arginines are more accessible to deuteration when the protein is bound to the lipid membrane, it is likely that they are involved in the structure of the hydrophilic channel. On the other hand, the nonaccessibility of the tyrosine residue suggests that this residue is turned toward the lipid phase and contributes in anchoring the protein into the membrane. The significant increase in protein helicity in the lipid environment has already been observed for the binding of other proteins and peptides to phospholipid membranes (*59*). Finally, the formation of a functional protein channel into the membrane is compatible with previous observations showing the absence of major changes in the lipid organization (*20*). These results confirm previous biological studies showing that the toxicity of purothionins is first based on changes in membrane permeability and not in a lytic activity. Lysis could be a secondary step that can be due to osmolarity changes leading to cell leakage. This phenomenon most likely occurred with liposomes containing large fluorescent molecules (*60*).

REFERENCES

1. Fernandez de Caleya, R., Hernandez-Lucas, C., Carbonero, P., and Garcia-Olmedo, F. (1976) Gene expression in alloploids: Genetic control of lipopurothionins in wheat, *Genetics 83*, 687−699.
2. Clore, G. M., Sukumaran, D. K., Gronenborn, A. M., Teeter, M. M., Whitlow, M., and Jones, B. L. (1987) Nuclear magnetic resonance study of the solution structure of α1-purothionin, *J. Mol. Biol. 193*, 571−578.
3. Stec, B., Rao, U., and Teeter, M. M. (1995) Refinement of purothionins reveals solute particles important for lattice formation and toxicity. Part 2: Structure of β-purothionin at 1.7 Å resolution, *Acta Crystallogr. D51*, 914−924.
4. Rao, U., Stec, B., and Teeter, M. M. (1995) Refinement of purothionins reveals solute particles important for lattice formation and toxicity. Part 1: α1-Purothionin revisited, *Acta Crystallogr. D51*, 904−913.
5. Clore, G. M., Nilges, M., Sukumaran, D. K., Brünger, A. T., Karplus, M., and Gronenborn, A. M. (1986) The three-dimensional structure of α1-purothionin in solution: Combined use of nuclear magnetic resonance, distance geometry and restrained molecular dynamics, *EMBO J. 5*, 2729−2735.
6. Teeter, M. M., Mazer, J. A., and l'Italien, J. (1981) Primary structure of the hydrophobic plant protein crambin, *Biochemistry 20*, 5437−5443.
7. Fernandez de Caleya, R., Gonzalez-Pascual, B., Garcia-Olmedo, F., and Carbonero, P. (1972) Susceptibility of phytopathogenic bacteria to wheat purothionins in vitro, *Appl. Microbiol. 23*, 998−1000.
8. Stuart, L. S., and Harris, T. H. (1942) Bactericidal and fungicidal properties of a crystalline protein isolated from unbleached wheat flour, *Cereal Chem. 19*, 288−300.
9. Coulson, E. J., Harris, T. H., and Axelrod, B. (1942) Effect on small laboratory animals of the injection of the crystalline hydrochloride of a sulfur protein from wheat flour, *Cereal Chem. 19*, 301−307.
10. Nakanishi, T., Yoshizumi, H., Tahara, S., Hakura, A., and Toyoshima, K. (1979) Cytotoxicity of purothionin-α on various animal cells, *Jpn. J. Cancer Res. 70*, 323−326.
11. Carrasco, L., Vazquez, D., Hernandez-Lucas, C., Carbonero, P., and Garcia-Olmedo, F. (1981) Thionins: Plant peptides that modify membrane permeability in cultured mammalian cells, *Eur. J. Biochem. 116*, 185−189.
12. Kramer, K. J., Klassen, L. W., Jones, B. L., Speirs, R. D., and Kammer, A. E. (1979) Toxicity of purothionin and its homologues of the tobacco hornworm, *Manduca sexta* (L.) (Lepidoptera: Sphingidae), *Toxicol. Appl. Pharmacol. 48*, 179−183.
13. Wada, K., Ozaki, Y., Matsubara, H., and Yoshizumi, H. (1982) Studies on purothionin by chemical modifications, *J. Biochem. 91*, 257−263.
14. Van Etten, C. H., Gagne, W. E., Robbins, D. J., Booth, A. N., Daxenbichler, M. E., and Wolff, I. A. (1969) Biological evaluation of *Crambe* seed meals and derived products by rat feeding, *Cereal Chem. 46*, 145−155.
15. Mattei, C., Elmorjani, K., Molgo, J., Marion, D., and Benoit, E. (1998) The wheat proteins puroindoline-a and α1-purothionin induce nodal swelling in myelinated axons, *NeuroReport 9*, 3803−3807.
16. Benoit, E., Elmorjani, K., Molgo, J., Marion, D., and Minic, J. (2002) Actions neuronales et musculaires de deux polypeptides de l'albumen de blé, in *Rencontres en toxinologie: Explorer, exploiter les toxines et maitriser les organismes producteurs* (Bon, C., Goudey-Perrière, F., Poulain, B., and Puiseux-Dao, S., Eds.) pp 79−80, Elsevier, Paris.
17. Hughes, P., Dennis, E., Whitecross, M., Llewellyn, D., and Gage, P. (2000) The cytotoxic plant protein, β-purothionin, forms ion channels in lipid membranes, *J. Biol. Chem. 275*, 823−827.
18. Llanos, P., Hentiquez, M., Minic, J., Elmorjani, K., Marion, D., Riquelme, G., Molgo, J., and Benoit, E. (2004) Neuronal and muscular alterations caused by two wheat endosperm proteins, puroindoline-a and α-purothionin, are due to ion pore formation, *Eur. Biophys. J. 33*, 283−284.
19. Huang, W., Vernon, L. P., Hansen, L. D., and Bell, J. D. (1997) Interactions of thionin from *Pyrularia pubera* with dipalmitoylphosphatidylglycerol large unilamellar vesicles, *Biochemistry 36*, 2860−2866.
20. Richard, J.-A., Kelly, I., Marion, D., Pézolet, M., and Auger, M. (2002) Interaction between β-purothionin and dimyristoylphosphatidylglycerol: A ^{31}P NMR and infrared spectroscopic study, *Biophys. J. 83*, 2074−2083.
21. Goormaghtigh, E., Cabiaux, V., and Ruysschaert, J.-M. (1994) Determination of soluble and membrane protein structure by Fourier transform infrared spectroscopy III. Secondary Structures, in *Subcellular Biochemistry: Physicochemical Methods in the Study of Biomembranes* (Hilderson, H. J., and Ralston, G. B., Eds.) pp 405−450, Plenum Press, New York.
22. Byler, D. M., and Susi, H. (1986) Examination of the secondary structure of proteins by deconvoluted Fourier-transform IR spectra, *Biopolymers 25*, 469−488.
23. Kauppinen, J. K., Moffatt, D. J., and Mantsch, H. H. (1981) Fourier self-deconvolution: A method for resolving intrinsically overlapped bands, *Appl. Spectrosc. 35*, 271−276.
24. Surewicz, W. K., and Mantsch, H. H. (1988) New insight into protein secondary structure from resolution-enhanced infrared spectra, *Biochim. Biophys. Acta 952*, 115−130.
25. Noda, I. (1990) Two-dimensional infrared (2D IR) spectroscopy: Theory and applications, *Appl. Spectrosc. 44*, 550−561.
26. Noda, I. (1993) Generalized two-dimensional correlation method applicable to infrared, Raman, and other types of spectroscopy, *Appl. Spectrosc. 47*, 1329−1336.
27. Noda, I., Dowrey, A. E., and Marcott, C. (1988) Spectrometer for measuring time-resolved infrared linear dichroism induced by a small-amplitude oscillatory strain, *Appl. Spectrosc. 42*, 203−216.

28. Noda, I. (1989) Two-dimensional infrared spectroscopy, *J. Am. Chem. Soc. 111*, 8116−8118.
29. Nabet, A., and Pézolet, M. (1997) Two-dimensional FT-IR spectroscopy: A powerful method to study the secondary structure of proteins using H−D exchange, *Appl. Spectrosc. 51*, 466−469.
30. Meskers, S., Ruysschaert, J.-M., and Goormaghtigh, E. (1999) Hydrogen−deuterium exchange of streptavidin and its complex with biotin by 2D-attenuated total reflection Fourier transform infrared spectroscopy, *J. Am. Chem. Soc. 121*, 5115−5122.
31. Ozaki, Y., Liu, Y., and Noda, I. (1997) Two-dimensional infrared and near-infrared correlation spectroscopy: Applications to studies of temperature-dependent spectral variations of self-associated molecules, *Appl. Spectrosc. 51*, 526−535.
32. Sefara, N. L., Magtoto, N. P., and Richardson, H. H. (1997) Structural characterization of β-lactalbumin in solution using two-dimensional FT mid-infrared and FT-near-infrared correlation spectroscopy, *Appl. Spectrosc. 51*, 536−540.
33. Schultz, C. P., Fabian, H., and Mantsch, H. H. (1998) Two-dimensional mid-IR and near-IR correlation spectra of ribonuclease A using overtones and combination modes to monitor changes in secondary structure, *Biospectroscopy 4*, S19−S29.
34. Fabian, H., Mantsch, H. H., and Schultz, C. P. (1999) Two-dimensional IR correlation spectroscopy: Sequential events in the unfolding process of the λ cro-V55C repressor protein, *Proc. Natl. Acad. Sci. U.S.A. 96*, 13153−13158.
35. Schultz, C. P., Barzû, O., and Mantsch, H. H. (2000) Two-dimensional infrared correlation analysis of protein unfolding: Use of spectra simulations to validate structural changes during thermal denaturation of bacterial CMP kinases, *Appl. Spectrosc. 54*, 931−938.
36. Paquet, M.-J., Laviolette, M., Pézolet, M., and Auger, M. (2001) Two-dimensional infrared correlation spectroscopy study of the aggregation of cytochrome *c* in the presence of dimyristoylphosphatidylglycerol, *Biophys. J. 81*, 305−312.
37. Filosa, A., Wang, Y., Ismail, A. A., and English, A. M. (2001) Two-dimensional infrared correlation spectroscopy as a probe of sequential events in the thermal unfolding of cytochromes *c*, *Biochemistry 40*, 8256−8263.
38. Yan, Y.-B., Wang, Q., He, H.-W., Hu, X.-Y., Zhang, R.-Q., and Zhou, H.-M. (2003) Two-dimensional infrared correlation spectroscopy study of sequential events in the heat-induced unfolding and aggregation process of myoglobin, *Biophys. J. 85*, 1959−1967.
39. Torrecillas, A., Corbalan-Garcia, S., and Gomez-Fernandez, J. C. (2004) An infrared spectroscopic study of the secondary structure of protein kinase Cα and its thermal denaturation, *Biochemistry 43*, 2332−2344.
40. Smeller, L., and Heremans, K. (1999) 2D FT-IR spectroscopy analysis of the pressure-induced changes in proteins, *Vib. Spectrosc. 19*, 375−378.
41. Murayama, K., Wu, Y., Czarnik-Matusewicz, B., and Ozaki, Y. (2001) Two-dimensional/attenuated total reflection infrared correlation spectroscopy studies on secondary structural changes in human serum albumin in aqueous solutions: pH-dependent structural changes in the secondary structures and in the hydrogen bondings of side chains, *J. Phys. Chem. B 105*, 4763−4769.
42. Wu, Y., Murayama, K., and Ozaki, Y. (2001) Two-dimensional infrared spectroscopy and principal component analysis studies of the secondary structure and kinetics of hydrogen−deuterium exchange of human serum albumin, *J. Phys. Chem. B 105*, 6251−6259.
43. Raussens, V., Ruysschaert, J.-M., and Goormaghtigh, E. (2004) Analysis of $^{1}H/^{2}H$ exchange kinetics using model infrared spectra, *Appl. Spectrosc. 58*, 68−82.
44. Griffiths, P. R., and Pariente, G. L. (1986) Introduction to spectral deconvolution, *Trends Anal. Chem. 5*, 209−215.
45. Goormaghtigh, E., Cabiaux, V., and Ruysschaert, J.-M. (1994) Determination of soluble and membrane protein structure by Fourier transform infrared spectroscopy. I. Assignments and model compounds, in *Subcellular Biochemistry: Physicochemical Methods in the Study of Biomembranes* (Hilderson, H. J., and Ralston, G. B., Eds.) pp 329−362, Plenum Press, New York.
46. Venyaminov, S. Y., and Kalnin, N. N. (1990) Quantitative IR spectrophotometry of peptide compounds in water (H_2O) solutions. I. Spectral parameters of amino acid residue absorption bands, *Biopolymers 30*, 1243−1257.
47. Chirgadze, Y. N., Fedorov, O. V., and Trushina, P. (1975) Estimation of amino acid residue side-chain absorption in the infrared spectra of protein solutions in heavy water, *Biopolymers 14*, 679−694.
48. Arrondo, J. L. R., Muga, A., Castresana, J., and Goni, F. M. (1993) Quantitative studies of the structure of proteins in solution by Fourier-transform infrared spectroscopy, *Prog. Biophys. Mol. Biol. 59*, 23−56.
49. Williams, R. W., and Teeter, M. M. (1984) Raman spectroscopy of homologous plant toxins: Crambin and α1- and β-purothionin secondary structures, disulfide conformation and tyrosine environment, *Biochemistry 23*, 6796−6802.
50. Hildebrandt, P. G., Copeland, R. A., and Spiro, T. G. (1988) Tyrosine hydrogen-bonding and environmental effects in proteins probed by ultraviolet resonance Raman spectroscopy, *Biochemistry 27*, 5426−5433.
51. Prendergast, F. G., Hampton, P. D., and Jones, B. (1984) Characteristics of tyrosinate fluorescence emission in α- and β-purothionins, *Biochemistry 23*, 6690−6697.
52. Dousseau, F., and Pézolet, M. (1990) Determination of the secondary structure content of proteins in aqueous solutions from their amide I and amide II infrared bands. Comparison between classical and partial least-squares methods, *Biochemistry 29*, 8771−8779.
53. Rothschild, K. J., Sanches, R., Hsiao, T. L., and Clark, N. A. (1980) A spectroscopic studic of rhodopsin α-helix orientation, *Biophys. J. 31*, 53−64.
54. Rothschild, K. J., and Clark, N. A. (1979) Polarized infrared spectroscopy of oriented purple membrane, *Biophys. J. 25*, 473−488.
55. Rothschild, K. J., and Clark, N. A. (1979) Anomalous amide I infrared absorption of purple membrane, *Science 204*, 311−312.
56. Czarnecki, M. A. (1998) Interpretation of two-dimensional correlation spectra: Science or art? *Appl. Spectrosc. 52*, 1583−1590.
57. Lefèvre, T., Arseneault, K., and Pézolet, M. (2004) Study of protein aggregation using two-dimensional correlation infrared spectroscopy and spectral simulations, *Biopolymers 73*, 705−715.
58. Evans, J., Wang, Y., Shaw, K., and Vernon, L. P. (1989) Cellular responses to *Pyrularia* thionin are mediated by Ca^{2+} influx and phospholipase A_2 activation and are inhibited by thionin tyrosine iodination, *Proc. Natl. Acad. Sci. U.S.A. 86*, 5849−5853.
59. Bechinger, B. (1999) The structure dynamics and orientation of antimicrobial peptides in membranes by multidimensional solid-state NMR spectroscopy, *Biochim. Biophys. Acta 1462*, 157−183.
60. Caaveiro, J. M. M., Molina, A., Rodriguez-Palenzuela, P., Goni, F. M., and Gonzalez-Manas, J. M. (1998) Interaction of wheat α-thionin with large unilamellar vesicles, *Protein Sci. 7*, 2567−2577.
61. Mantsch, H. H., Perczel, A., Hollosi, M., and Fasman, G. D. (1993) Characterization of β-turns in cyclic hexapeptides in solution by Fourier transform IR spectroscopy, *Biopolymers 33*, 201−207.
62. Mendelsohn, R., and Mantsch, H. H. (1986) Fourier transform infrared studies of lipid−protein interaction, in *Progress in Protein−Lipid Interactions* (Watts, A., and De Pont, J. J. H. H. M., Eds.) pp 103−146, Elsevier, New York.
63. Bahng, M. K., Cho, N. J., Park, J. S., and Kim, K. (1998) Interaction of indolicidin with model lipid bilayers: FTIR-ATR spectroscopic study, *Langmuir 14*, 463−470.

BI048443T